RSC Advances

PAPER

View Article Online
View Journal | View Issue

Open Access Article. Published on 19 July 2023. Downloaded on 1/12/2026 11:23:45 PM.
This article is licensed under a Creative Commons Attribution-NonCommercial 3.0 Unported Licence.

Check for updates

Cite this: *RSC Adv.*, 2023, **13**, 21643

# A binary composite $La(OH)_3$@$Ni(OH)_2$ nanomaterial on carboxyl graphene for an efficient hybrid supercapacitor electrode

Dianyuan Zheng,[ac] Chengxiang Sun,*[ab] Rongbin Yao,*[a] Jinli Li,[a] Yuhang Zheng,[d] Jianhong Zhu[b] and Cheng Liu[e]

In this work, we present a binary composite of $La(OH)_3$@$Ni(OH)_2$ on carboxyl graphene (La@Ni/CG) as an electrode material. The layered La@Ni/CG double hydroxides (LDHs) were synthesized by a simple electrodeposition method in which $La(OH)_3$ nanoparticles were first adsorbed onto carboxyl graphene and then coated with $Ni(OH)_2$, with different particle shapes due to the large pH change near the cathodic region. Scanning electron microscopy (SEM), X-ray diffraction (XRD), X-ray photoelectron spectroscopy (XPS), cyclic voltammetry (CV) and galvanostatic charge–discharge (GCD) were used to characterise the as-prepared La@Ni/CG composite. These results showed that the La@Ni/CG composite exhibited improved electrochemical properties, including large specific capacitance (1334.7 F $g^{-1}$ at 1.4 A $g^{-1}$) and capacity retention of 90.6% even after 3000 cycles, and excellent rate capability. The improved electrochemical performance of the composite can be attributed to the synergistic effect of surface adsorption and conductive pathways provided by the multiple active species (Ni, La and C) in the La@Ni/CG composite. The results presented in this work provide advances in the efficient design of nanomaterial based electrochemical energy storage devices.

Received 12th May 2023
Accepted 25th June 2023

DOI: 10.1039/d3ra03151a

rsc.li/rsc-advances

## 1. Introduction

In recent years, the development of novel materials for electrochemical energy storage electrodes have attracted tremendous focus. Up to now, graphene and graphene-based materials are regarded as promising candidates for electrochemical energy storage electrodes, due to its large surface area, excellent electrical conductivity and excellent mechanical stability.[1–5] However, their energy density is still far from meeting the requirements of practical applications. Recently, layered $Ni(OH)_2$ has gained good chemical stability, low cost, and excellent electrochemical properties.[6,7] Even if $Ni(OH)_2$ is stable under harsh working conditions (alkaline environment and wide range of temperatures), the poor conductivity, reduced capacitance and low cycling stability of $Ni(OH)_2$-based electrodes still limits their commercial applications in electronic equipment.[8]

To address these issues, researchers have attempted to dope the material with suitably selected cations such as Ag, Mn, Co, Zn, Al and Y to induce artificial defects.[9–15] Among these, the incorporation of Ag dopants into $Ni(OH)_2$ can greatly increase its electrical conductivity due to the increase in chemical activity of the Ag dopants, resulting in the improved the charge transport mechanism and the decrease of resistivity. Mn doping in $Ni(OH)_2$ would effectively improve its electrochemical stability by reducing the crystallite size of $Ni(OH)_2$ and forming $Mn^{2+}$ ions, thereby facilitating the transfer of ions and electrons to reduce the reaction barriers of electrochemical processes. $ANiO_3$ (A = La, Ce) synthesized by the co-precipitation method, exhibit high surface area and good electrical conductivity, making it suitable for supercapacitor applications.[16] Since $LaNiO_3$ is usually formed at 650 °C, the metal current collector may become passivated under such high temperature, which could reduce the charge storage capacity of $LaNiO_3$. In addition, the $LaNiO_3$ is unstable at high temperature, resulting in changes in $LaNiO_3$ structure.

Compared with bare $Ni(OH)_2$, $Ni(OH)_2$-based electrodes possess significant improvements in the electrochemical performance. However, the cycling stability of these electrodes was limited to 500 cycles, indicating that further research is needed to improve the cycling stability of these electrodes. To further improve the electrical conductivity and cycling stability of $Ni(OH)_2$-based electrodes, some researchers have coupled them with carbon nanotubes, graphene,[17–23] transition metal

[a]Institute for Clean Energy & Advanced Materials, Lianyungang Normal College, Lianyungang 222006, China
[b]College of Energy and Electrical Engineering, Hohai University, Nanjing 210098, China. E-mail: chengxsun@hhu.edu.cn
[c]State Key Laboratory of Pharmaceutical Biotechnology, Department of Biochemistry, Nanjing University, Nanjing 210093, China
[d]State Grid Jiangsu Electric Power Engineering Consulting Co., Ltd, Nanjing, Jiangsu 210008, China
[e]College of Electrical Engineering, Zhejiang University, Hangzhou 310027, China

© 2023 The Author(s). Published by the Royal Society of Chemistry

Open Access Article. Published on 19 July 2023. Downloaded on 1/12/2026 11:23:45 PM. This article is licensed under a Creative Commons Attribution-NonCommercial 3.0 Unported Licence.

oxides,[24] polyaniline,[25,26] and polypyrrole.[27] Nowadays, there are various methods to prepare these composite electrodes, including spin-coating technique,[28] hydrothermal method,[29] electrospinning method,[30] and sol–gel method,[31] and so on. Especially, the electrochemical deposition method has been found to be advantageous to electro synthesize a wide range of materials on complex shaped conductive substrates,[32,33] in which the shape and thickness of the materials can be easily adjusted by controlling the voltage, current and deposition time.

Based on this, we developed a binary composite of $Ni(OH)_2$ and $La(OH)_3$ supported on carboxyl graphene (La@Ni/CG) as electrode for electrochemical energy storage, through a simple electrodeposition method. The incorporation of La dopants can greatly enhance its electrical conductivity, while CG can improve its electrochemical stability. In addition, the combination of $Ni(OH)_2$ with CG would provide high surface area, making it suitable for use in electrochemical energy storage applications. As a result, the La@Ni/CG electrode exhibited large specific capacitance (1334.7 F $g^{-1}$ at 1.4 A $g^{-1}$) and high capacity retention of 90.6% even after 3000 cycles, and excellent rate capability.

## 2. Experimental methods

### 2.1. Materials

Analytical grade $La(NO_3)_3$, $Ni(NO_3)_2$, anhydrous ethanol and acetone were purchased from China National Pharmaceutical Group (Shanghai). Graphene oxide was purchased from Jiangsu Xianfeng Nanometer Co., Ltd (Nanjing) without further purification before use. Foam nickel (NF) was purchased from Kejing Electronics (Shenzhen) Co., Ltd. Before use, the foam nickel (square 1 × 2 cm) was ultrasonically treated with acetone and anhydrous ethanol for 5 min each to remove possible organic contaminants, and then vacuum dried at 80 °C for standby.

### 2.2. Material characterization

The sample was analyzed using X-ray diffractometer (Bruker D8 Advance) with Cu-Kα ($\lambda = 0.15406$ nm) at the range of 10° to 80°. The morphology and composition of the samples were analyzed by field emission scanning electron microscopy (SEM, HITACHI S-4800, Japan) (EDS, Thermo Scientific, United States) and transmission electron microscope (TEM, FEI Tecnai G2 F20 microscope, USA). XPS measurement was performed on Al Kα with monochrome alpha radiation ($h\nu$ = 1486.6 eV) (Escalab 250Xi photoelectron spectrometer, USA).

### 2.3. Electrode preparation and electrochemical measurement

The typical electrode material was obtained by cathodic electrodeposition from a 100 mM $Ni(NO_3)_2$ solution containing 0.1 mg $mL^{-1}$ carboxymethyl graphene (excellent dispersion of 0.1 mg $mL^{-1}$ carboxysilyl graphene) additive and a 10 mM $La(NO_3)_3$ solution containing 0.1 mg $mL^{-1}$ carboxymethyl graphene additive. La@Ni/CG electrodes were prepared by applying 5 mA to electrodeposition in lanthanum nitrate solution for 300 s, then transferring to nickel nitrate solution and applying 9 mA to continue electrodeposition for 600 s. Nickel nitrate or lanthanum nitrate was used as electrodeposition solutions for $Ni(OH)_2$ and $La(OH)_3$ electrodes, respectively. After electrodeposition, the nickel foam was washed with deionized water for 5 min to remove residual liquid and then vacuum dried at 80 °C for 1 h to stand. The change in mass before and after the electrodeposition experiment was used to calculate the load of active material on the electrode. The as-prepared electrodes were called as La@Ni/CG, $Ni(OH)_2$/CG and $La(OH)_3$/CG.

Three electrode systems were used to investigate the electrochemical properties of La@Ni/CG, $Ni(OH)_2$/CG and $La(OH)_3$/CG electrode materials. The as-prepared electrode was used as the working electrode, the platinum plate as the counter electrode, Hg/HgCl as the reference electrode and 3 M KOH as the electrolyte. Electrochemical impedance spectroscopy (EIS) measurement was performed in the frequency range of 100 kHz to 0.01 Hz with an amplitude of 5 mV. Cyclic voltammetry (CV) was measured at different scan rates, with a potential window of 0–0.60 V. Cyclic voltammetry (CV), constant current charge/discharge (GCD) and electrochemical resistance spectroscopy (EIS) measurements were all performed using a CHI 660E (Shanghai Chenhua Instruments Co.) electrochemical workstation.

The specific capacitance of the electrode was calculated using the following equation:

$$C_s = \frac{1}{\nu \cdot m \cdot \Delta V} \int_{V_0}^{V_0+\Delta V} i \mathrm{d}V \tag{1}$$

$$C_s = \frac{i \times \Delta t}{m \times \Delta V} \tag{2}$$

where $C_s$ (F $g^{-1}$) is the specific capacitance, $i$ (mA) is the discharge current, $t$ (s) is the discharge time, $\nu$ (mV $s^{-1}$) is the scanning rate, $m$ is the mass of the active material, and $\Delta V$ (V) is the discharge potential window (excluding potential drop).

## 3. Results and discussion

Scheme 1 shows the possible reaction mechanism for the deposition of layered La@Ni/CG double hydroxides (LDHs) in a nitrate electrolytic bath. The nitrate ions ($NO_3^-$) in the electrolyte are reduced at the cathode to form ammonium ions ($NH_4^+$) and hydroxide ions

$$NO_3^- + 7H_2O + 8e^- \rightarrow NH_4^+ + 10OH^- \tag{3}$$

The local increase in pH due to the production of hydroxyl ions according to according to eqn (3), leads to the precipitation of the rare earth hydroxide near the cathodic region as of the rare earth metal hydroxide, such as:

$$La^{3+} + 3OH^- \rightarrow La(OH)_3\downarrow \tag{4}$$

$$Ni^{2+} + 2OH^- \rightarrow Ni(OH)_2\downarrow \tag{5}$$

 © 2023 The Author(s). Published by the Royal Society of Chemistry

Open Access Article. Published on 19 July 2023. Downloaded on 1/12/2026 11:23:45 PM.
This article is licensed under a Creative Commons Attribution-NonCommercial 3.0 Unported Licence.

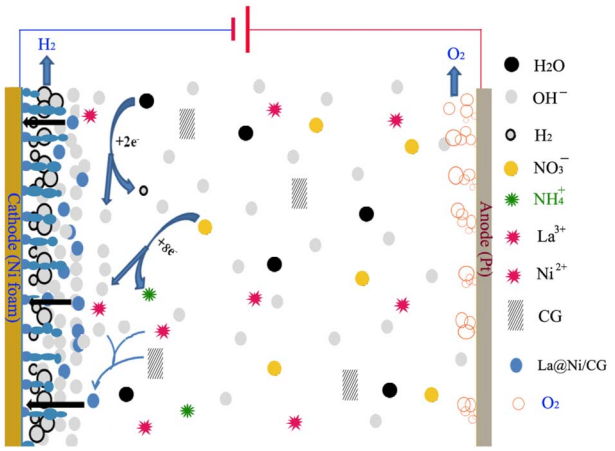


Scheme 1 The mechanism of electrodeposition reactions.

However, different electrodeposition currents produce $La(OH)_3$ with different particle shapes due to the large change in pH near the cathodic region. In addition, the hydrogen produced by the cathode also has a significant effect on the shape of the material. At the same time, the presence of $La(OH)_3$ on the electrode surface promotes the deposition of $Ni(OH)_2$ on the cathode surface, forming LDHs composites. In the presence of carboxylic acid-based graphene additives, carboxyl groups can interact with metal hydroxide particles to influence their growth and aggregation, and carboxymethyl-based graphene sheets or nitrate ions can also interact with LDH to form hybrid composites. Overall, the formation of LDHs in nitrate electrolytic bath involves a complex interplay of various electrochemical and chemical processes, and the exact mechanism may depend on the specific conditions of the electrolysis.

### 3.1. Material characterization of the as-prepared samples

The morphology of as-prepared samples was obtained by using SEM and TEM. Fig. 1a shows that the electrodeposited NF exhibits the surface, which is conducive to deposition. Fig. 1b and c indicated that $La(OH)_3$/CG particles were successfully deposited on NF. The $La(OH)_3$/CG particles displayed nanorod structure, which is interconnected and woven into sheet-like formations with the length of 100–500 nm and diameter of 50–200 nm.

The SEM images of the $Ni(OH)_2$/CG are shown in Fig. 1d and e. The ultrathin $Ni(OH)_2$/CG nanosheets are uniformly deposited on the nickel foam. Fig. 1e and f indicate that the $Ni(OH)_2$/CG nanoflakes exhibit lamellar structure with the outer diameter of 10–20 nm. The vertical growth of the nanosheets also allows for efficient electron and ion transport, further enhancing their performance. In addition, the interconnected structure enhances the stability and durability of the nanoparticles.

The SEM images in Fig. 1g–i show the nanostructures of $Ni(OH)_2$ and $La(OH)_3$ assembled into tight interconnections, forming villus-like structures. These nanoarrays are stacked to form a coiled structure of nanorods and nanosheets with various voids, which may be due to the generated gas during electrodeposition process. These voids are conducive to ion transport and reaction with the electrode surface. TEM images of La@Ni/CG (Fig. 1j) and insert SAED pattern was obtained by scraping the surface of the nickel foam. The accurate lattice fringes (Fig. 1k and l) were calculated to be 0.25 nm and 0.38 nm, which are contributing to the (100) of $Ni(OH)_2$ and (101) of $La(OH)_3$. The EDS element mapping images indicated the homogeneous distribution of the elements of La, Ni, O and C, where the C is due to the addition of carboxymethyl graphene (Fig. 1m).

Overall, the SEM images analysis confirms that La@Ni/CG exhibit highly porous and interconnected structure. The alkaline environment during electrodeposition and the decomposition of electrolytic water plays an important role in the formation of the nanoflakes. The small size of the villus-like structures, as well as the interconnected structure, contribute to the high performance, stability, and durability of the material.

The XRD analysis show that the $Ni(OH)_2$/CG and $La(OH)_3$/CG samples with different diffraction patterns, and the peaks observed in the spectrum of the composite material, La@Ni/CG, can be attributed to both phases. The presence of $La(OH)_3$ nanocrystals was confirmed by the peaks observed at 27.9°, 39.5°, 48.5°, 56.2°, 65.1°, 70.2°, and 77.4°.[34] The diffraction peaks at 19.2°, 33.0°, 38.5°, 59.0°, and 62.7° are assigned to the (001), (100), (101), (110), and (111) planes of cubic $Ni(OH)_2$,[35] respectively. The peak located at 27.9° in the XRD spectrum of the La@Ni/CG sample can be attributed to the low concentration of lanthanum ions wrapped in the nickel ion layer, resulting in poor crystallization. While the diffraction peak intensities of La@Ni/CG decreased slightly compared to $Ni(OH)_2$/CG, which was attributed to the addition of carboxyl graphene (Fig. 2a).

EDS analysis is a technique used to determine the elemental composition of a material. In this case, the EDS analysis confirmed the presence of Ni, O, C, and La in the prepared sample (Fig. 2b), which is consistent with the expected composition based on the synthesis method used, which is consistent with the EDS mapping mode analysis. The EDS mapping mode analysis also confirmed the distribution of these elements throughout the sample, which is important in determining the homogeneity of the composite material.

The vibrating atoms of $Ni(OH)_2$/CG, $La(OH)_3$/CG and La@Ni/CG were studied by FTIR technique. Fig. 2c shows the FTIR spectrum of the samples. The $Ni(OH)_2$/CG sample shows characteristic peaks at 3439, 1631, 1482, 1384 and 522, 462 $cm^{-1}$. The $La(OH)_3$/CG sample shows characteristic peaks at 3442, 1477, 1384 and 849, 645 $cm^{-1}$. The La@Ni/CG sample shows characteristic peaks at 3441, 1632, 1484, 1383 and 640, 521, 469 $cm^{-1}$. As shown in Fig. 4c, the peak at 3439–3442 $cm^{-1}$ represents the hydroxide group. The absorption peaks around 1383–1632 $cm^{-1}$ are recognised as O–H, C–C, C–O bending vibrations combined with Ni and La atoms. The peak at 462–849 $cm^{-1}$ corresponds to the metal–oxygen (Ni–O, La–O) vibrational modes of the LDHs compound. There are

Open Access Article. Published on 19 July 2023. Downloaded on 1/12/2026 11:23:45 PM.
This article is licensed under a Creative Commons Attribution-NonCommercial 3.0 Unported Licence.

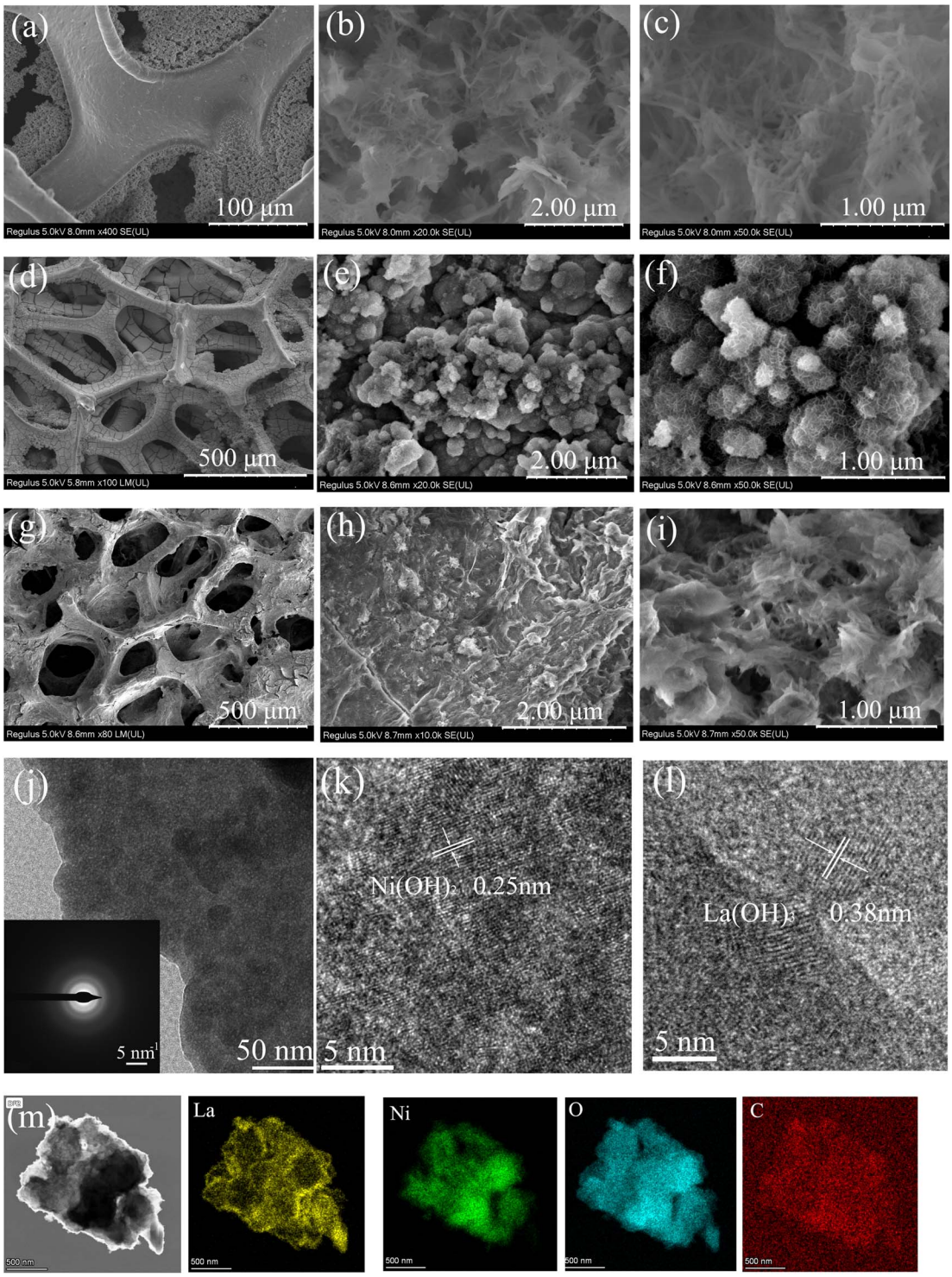


Fig. 1 SEM images of $La(OH)_3$/CG (a)–(c), $Ni(OH)_2$/CG (d)–(f) and La@Ni/CG (g)–(i); TEM images of La@Ni/CG (j) and insert SAED pattern; HRTEM images of La@Ni/CG (k) and (l); TEM images of La@Ni/CG and corresponding mappings of La, Ni, O and C (m).

two bands at 640, 521, 469 $cm^{-1}$ in the La@Ni/CG sample, which are sharp and of low intensity, corresponding to Ni–O and La–O peaks. The results indicate the existence of –OH groups and Ni–O and La–O bonds for $Ni(OH)_2$ and $La(OH)_3$ nanoparticles, and carboxymethyl-based graphene sheets or nitrate ions can also interact with LDH to form hybrid composites, indicating the successful construction of La@Ni/CG nanoparticles.

Overall, the XRD, EDS and FTIR results provide evidence for the successful synthesis of La@Ni/CG material and the presence of $La(OH)_3$ nanocrystals in the composite structure.

 © 2023 The Author(s). Published by the Royal Society of Chemistry

Open Access Article. Published on 19 July 2023. Downloaded on 1/12/2026 11:23:45 PM.
This article is licensed under a Creative Commons Attribution-NonCommercial 3.0 Unported Licence.

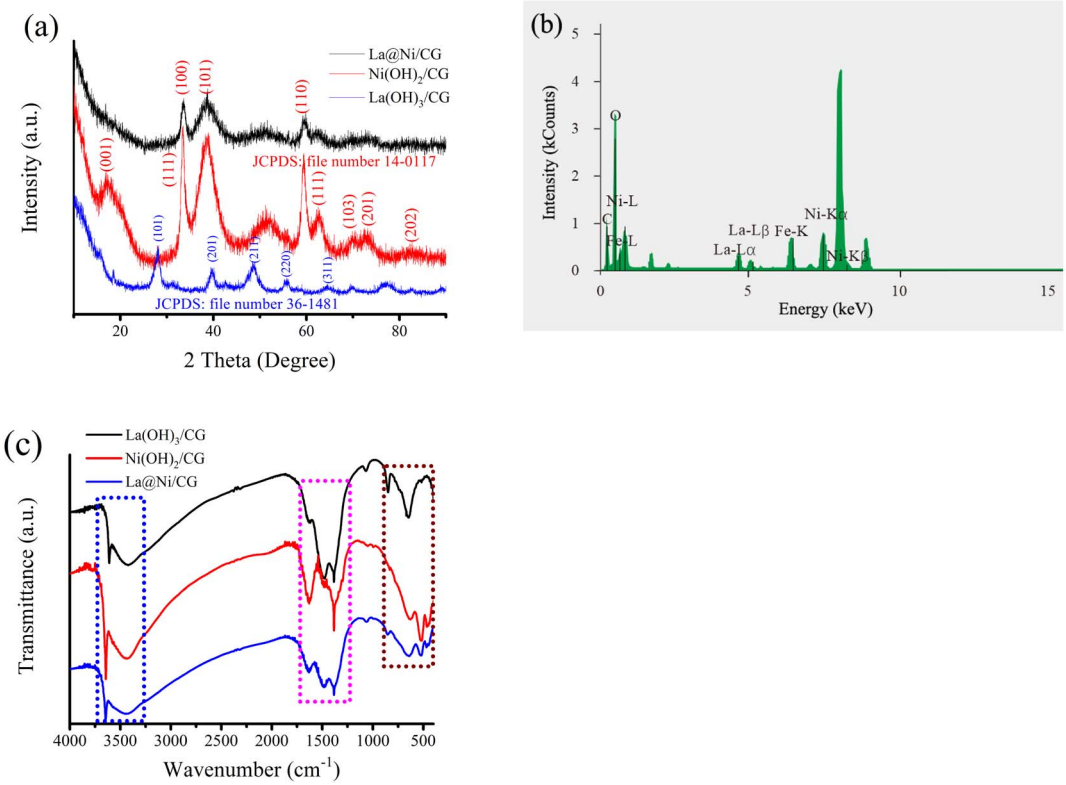


Fig. 2 (a) XRD patterns of all samples; (b) EDS pattern of the La@Ni/CG; (c) FTIR spectrums of $Ni(OH)_2$/CG, $La(OH)_3$/CG and La@Ni/CG nanoparticles.

The XPS measurement was employed to investigate elemental composition of La@Ni/CG (Fig. 3). As shown in Fig. 3b, there are $Ni^0$ (852.3 eV), $Ni^{2+}$–O (853.2 eV), and $Ni^{2+}$–OH (855.9 eV, 865.2 eV) components in the high-resolution Ni 2p XPS.[36] The information suggests that nickel ions have different oxidation states in the composite, which could affect the reactivity, catalytic activity, and potential applications in energy storage and conversion. In addition, the La 3d spectral region shows further splitting of the spin orbital component. Although lanthanum ($La^{3+}$) has only one chemical state, the peaks at 835.4 and 852.4 eV are attributed to La $3d_{5/2}$ and La $3d_{3/2}$.[37] The distance between the two peaks of La $3d_{5/2}$ is about 3.3 eV, which is close to 3.9 eV of $La(OH)_3$. It is noteworthy that the La@Ni/CG material has the displacement of Ni $2p_{3/2}$ main peak. The blue shift of binding energy is related to the d band shift, which is a sign of electrical activity. The C 1s and O 1s spectra also provide information about oxygenated materials. The C 1s band is deconvoluted into four peaks, with binding energies of 284.6, 286.5, 288.5, and 290.5 eV, corresponding to C–C, C–O, O=C–H, and O=C–O bonds. In addition, the O 1s core level spectrum is decomposed into two components with binding energies of 530.8 and 532.2 eV, which are related to $O^{2-}$ and bridging hydroxyl groups. This information suggests that the encapsulation of nickel and lanthanum by carboxymethyl graphene has a significant effect on the electronic and chemical properties of the material. The presence of multiple valence states of nickel and the spin–orbit splitting of lanthanum indicate that the material is highly reactive and may have potential applications in catalysis and energy storage.

Overall, the XPS measurement provides valuable information about the chemical state and composition of the La@Ni/CG composite, revealing the presence of multiple valence states of nickel and the spin–orbit splitting of lanthanum. The blue shift of binding energy in the Ni $2p_{3/2}$ peak indicates its electrical activity, while the analysis of the C 1s and O 1s core level spectra further confirms the presence of oxygen-containing substances in the material.

### 3.2. Electrochemical performance

CV measurement was performed at different scan rates ranging from 0 to 0.60 V (*vs.* Hg/HgCl) to investigate the capacitive properties of the samples (Fig. 4). The effect of addition of carboxymethyl graphene during electrodeposition on the mass specific capacitance of the original samples of $La(OH)_3$ and $Ni(OH)_2$ samples, as shown in Fig. 4a. The results indicate that carboxymethyl graphene is an effective additive in improving the mass specific capacitance. Fig. 4b shows that the mass specific capacitance of La@Ni/CG electrode materials with the mass ratio of $La(OH)_3$ in the composite. The specific capacitance increases and then decreases with the $La(OH)_3$ ratio increases. The main contribution to the specific capacitance of the material is observed when the mass ratio of $La(OH)_3$ is 10%. This ratio can be precisely controlled by the electrodeposition conditions.

Open Access Article. Published on 19 July 2023. Downloaded on 1/12/2026 11:23:45 PM.
This article is licensed under a Creative Commons Attribution-NonCommercial 3.0 Unported Licence.

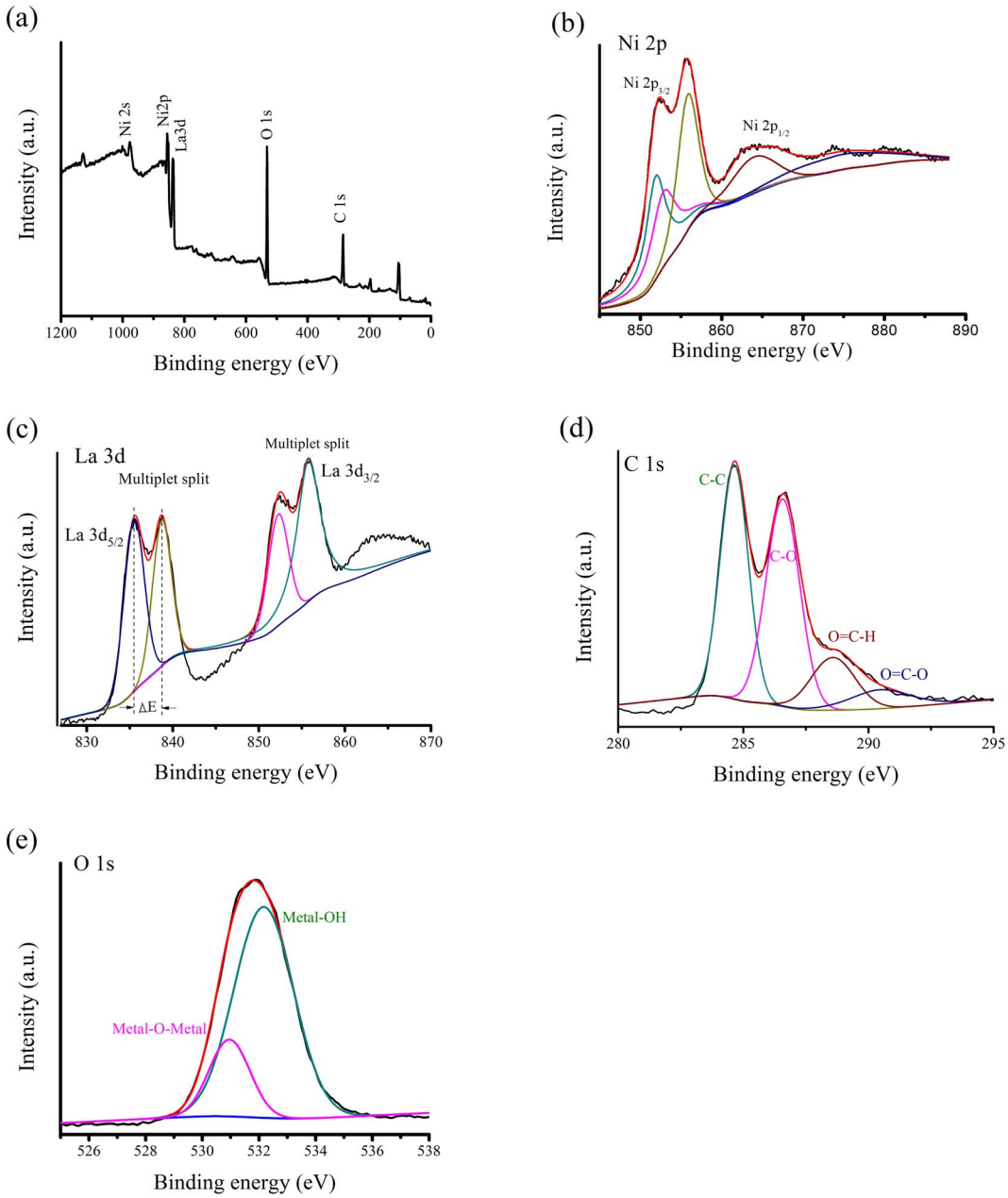


Fig. 3 XPS survey spectra of La@Ni/CG. (a) Survey spectrum; (b) Ni 2p; (c) La 3d; (d) O 1s and (e) C 1s.

Fig. 4c showed the CV curves of the $La(OH)_3$/CG sample at a scan rate of 5 mV $s^{-1}$, the oxidation peak of the current sample occurs at about 0.39 V, indicating the conversion of $La^{3+}$ to $La^{4+}$, while the reduction peak occurs at about 0.29 V. The small potential difference between the two peaks, which is around 0.1 V, indicates excellent reversibility. The oxidation peak of the $Ni(OH)_2$/CG sample appears at about 0.45 V, indicating the conversion of $Ni^{2+}$ to $Ni^{3+}$, while the reduction peak appears at about 0.21 V. The potential difference between the oxidation and reduction peaks of the $Ni(OH)_2$/CG material is about 0.2 V, and its reversibility is lower compared to that of $La(OH)_3$/CG. The oxidation peak of the La@Ni/CG material is observed at about 0.41 V and 0.22 V, and the potential difference between the two materials is within this range. Furthermore, the current density of the La@Ni/CG material at the redox peak is significantly higher than that of the $La(OH)_3$/CG and $Ni(OH)_2$/CG samples, indicating a superior charge storage capacity of La@Ni/CG material. The LDHs lattice inevitably leads to the alteration of the crystal $La(OH)_3$ and $Ni(OH)_2$, making the $Ni^{2+}$ species more reactive. Meanwhile, a new small oxidative peak appears in the potential range of 0.45 V to 0.47 V. It is suggested that the capacitance performance of the material is enhanced by the interaction between $La(OH)_3$ and $Ni(OH)_2$. Fig. 4c shows that all curves show two distinct and prominent redox peaks in each scan. These peaks are attributed to the interconversion between $Ni(OH)_2$ and NiOOH, LaOOH and $LaO(OH)_3^-$ according to the following reaction.

 © 2023 The Author(s). Published by the Royal Society of Chemistry

Open Access Article. Published on 19 July 2023. Downloaded on 1/12/2026 11:23:45 PM.
This article is licensed under a Creative Commons Attribution-NonCommercial 3.0 Unported Licence.

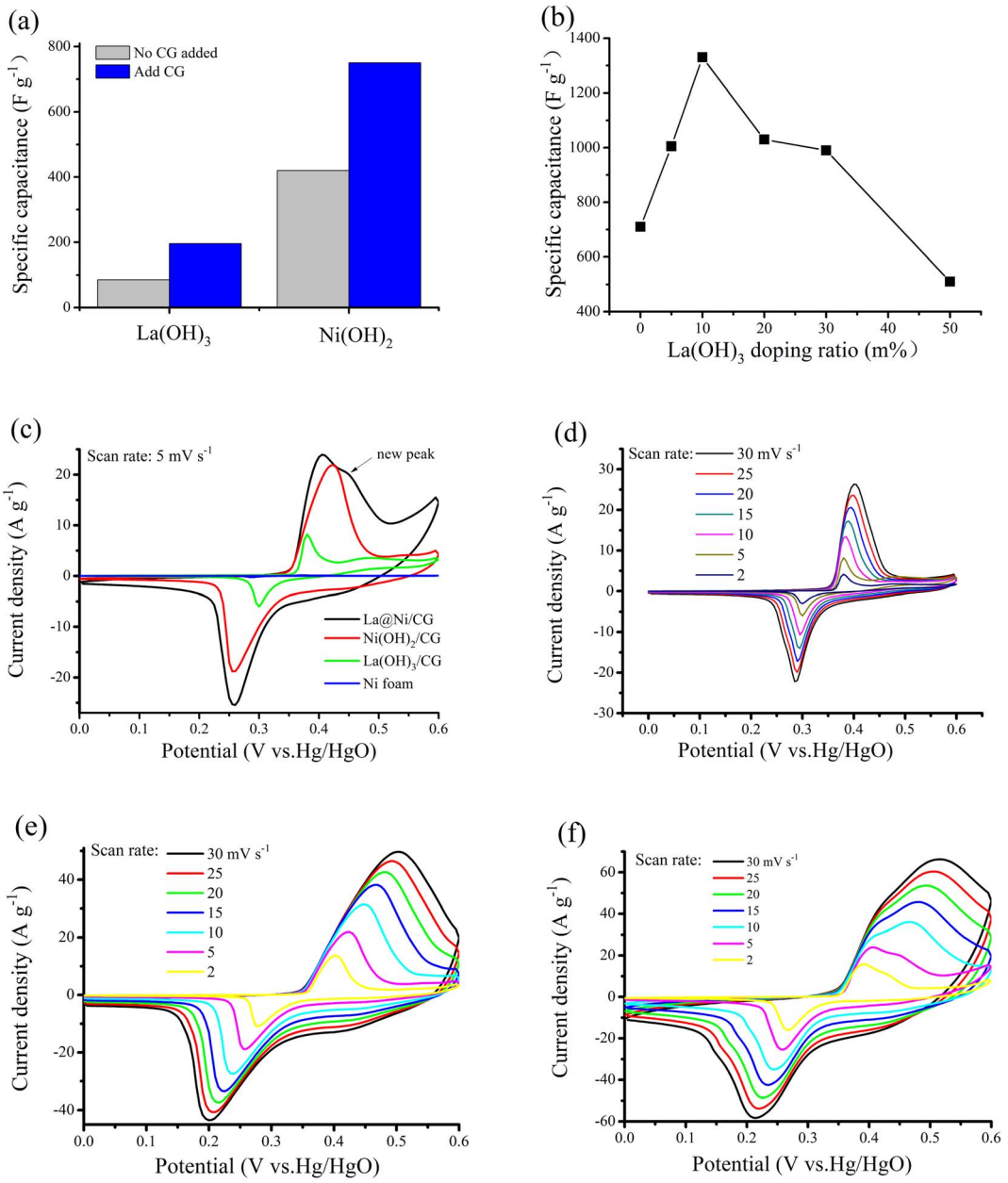


Fig. 4 (a) Changes in specific capacitance of $La(OH)_3$ and $Ni(OH)_2$ after addition of carboxymethyl graphene; (b) effect of $La(OH)_3$ on comparative capacity; (c) CV curves of $La(OH)_3$/CG, $Ni(OH)_2$/CG and La@Ni/CG at a scan rate of 5 mV $s^{-1}$; (d) CV curves of $La(OH)_3$/CG at different scan rates; (e) CV curves of $Ni(OH)_2$/CG at different scan rates; (f) CV curves of La@Ni/CG at different scan rates.

$$Ni(OH)_2 + OH^- \leftrightarrow NiOOH + H_2O + e^- \quad (6)$$

$$LaOOH + 2OH^- \leftrightarrow LaO(OH)_3^- + e^- \quad (7)$$

In addition, the mass specific capacitance of $La(OH)_3$/CG, $Ni(OH)_2$/CG and La@Ni/CG are obtained according to the corresponding CV curves, respectively. The CV curves are shown in Fig. 4d–f for different scanning rates. At the scan rate of 2 mV $s^{-1}$, the mass specific capacitance is 190, 760 and 1220 F $g^{-1}$ for $La(OH)_3$, $Ni(OH)_2$ and La@Ni/CG, respectively.

The GCD measurement was used to investigate the electrochemical performance of $Ni(OH)_2$/CG and La@Ni/CG, with different current densities (1 to 16 A $g^{-1}$) and potential windows (0–0.5 V). All GCD curves are non-linear, indicating pseudocapacitive behavior, which is consistent with the results of CV. The symmetrical charge and discharge curves with no significant *iR* drop indicate good capacitance performance and excellent reversibility of the Faraday redox reaction. The oxidation and reduction processes are responsible for the obvious charge and discharge platforms at around 0.35 V and 0.25 V. The specific capacitance of $Ni(OH)_2$/CG and La@Ni/CG are shown in Fig. 5b and d. As we can see that with the current density increases, the specific capacitance decreases. The specific capacitance of $Ni(OH)_2$/CG decreases (740.1, 600.2,

Open Access Article. Published on 19 July 2023. Downloaded on 1/12/2026 11:23:45 PM.
This article is licensed under a Creative Commons Attribution-NonCommercial 3.0 Unported Licence.

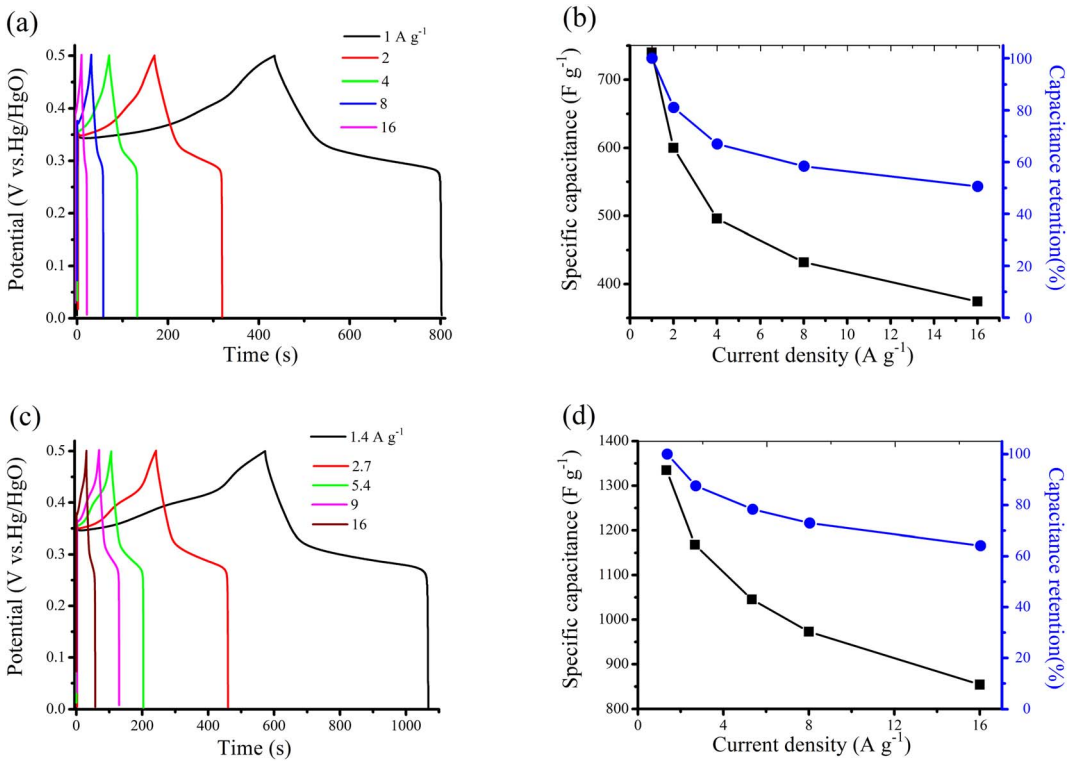


Fig. 5 (a) and (c) GCD of $Ni(OH)_2$/CG and La@Ni/CG at different current densities; (b) and (d) specific capacitance and capacitance retention of $Ni(OH)_2$/CG and La@Ni/CG at various current densities.

496.2, 432.5, and 374.4 F $g^{-1}$) as the current densities increase (1, 2, 4, 8, and 16 A $g^{-1}$). Furthermore, the capacitance retention is reported to be 50.6%, indicating that the electrode material retains approximately half of its original capacitance over the range of current densities. These results suggest that the electrode material may be suitable for applications with high capacitance at low current densities. For the La@Ni/CG, the specific capacitance is 1334.7, 1068.1, 1045.3, 1114 and 854.4 F $g^{-1}$ at the corresponding current densities of 1.4, 2.7, 5.4, 9 and 16 A $g^{-1}$, respectively, and the capacitance retention is 64.1%. Overall, these results suggest that the electrode material may be suitable for applications requiring high capacitance at intermediate current densities. However, its capacitance may decrease significantly at higher current densities. The relatively high capacitance retention rate suggests that the material with excellent long-term stability. Compared to $Ni(OH)_2$/CG, the charge storage capacity of La@Ni/CG is better than that of $Ni(OH)_2$/CG, which is probably due to the presence of $La^{3+}$ ions. These ions are thought to activate the active site of the $Ni(OH)_2$ material, resulting in an enhanced redox reaction. Clearly, the electrochemical properties of La@Ni/CG, including mass loading, specific capacitance and cycling stability, are highly competitive with recent reports of La-doped supercapacitor electrodes, as shown in Table 1.[9,38–44]

The excellent electrochemical performance of the samples may be ascribed to the active site of the $Ni(OH)_2$ activated by $La^{3+}$. The activation can be confirmed by the curve of peak current ($i$) *versus* scan rate ($\nu^{1/2}$), as shown in Fig. 6a. It also suggests that the addition of 10% $La(OH)_3$ can result in a high specific capacitance of the La@Ni/CG composite. This improvement can be quantified as 37% increase in the CV curve area (Fig. 4c). This suggests that the anode peak current and the square root of the scan rate in the

Table 1 Electrochemical performance of the La-doped three-electrode electrodes of a supercapacitor as reported

| Materials | Synthesis method | Capacitance (F $g^{-1}$) | Cycling ability | Ref. |
|---|---|---|---|---|
| La@Ni/CG | Electrodeposition | 1334.7 at 1.4 A $g^{-1}$ | 90.6% (3000 cycle) | This work |
| La-doped $Ni(OH)_2$ | Electrodeposition | 840 at 0.1 A $g^{-1}$ | — | 38 |
| $La_2O_3$–NiO | Hydrothermal method | 564 at 1.0 A $g^{-1}$ | 93.4% (2000 cycle) | 39 |
| $LaNiO_3$/NiO | Electrospinning method | 942 at 0.5 A $g^{-1}$ | 90% (1000 cycle) | 40 |
| La–$Ni(OH)_2$ | Hydrothermal method | 1510.7 at 1.0 A $g^{-1}$ | 89.3% (2000 cycle) | 41 |
| $La(CoCrFeMnNiAl_{0.5})_{1/5.5}O_3$ | Coprecipitation method | 353.6 at 1.0 A $g^{-1}$ | 88.6% (2000 cycle) | 42 |
| $LaMnO_3$@$NiCo_2O_4$/carbon cloth | Electrodeposition | 942 at 1.0 A $g^{-1}$ | — | 43 |
| CSD-$LaNiO_3$/NiO | Chemical precipitation method | 326.8 at 1.0 A $g^{-1}$ | 96.1% (3000 cycle) | 44 |

 © 2023 The Author(s). Published by the Royal Society of Chemistry

Open Access Article. Published on 19 July 2023. Downloaded on 1/12/2026 11:23:45 PM.
This article is licensed under a Creative Commons Attribution-NonCommercial 3.0 Unported Licence.

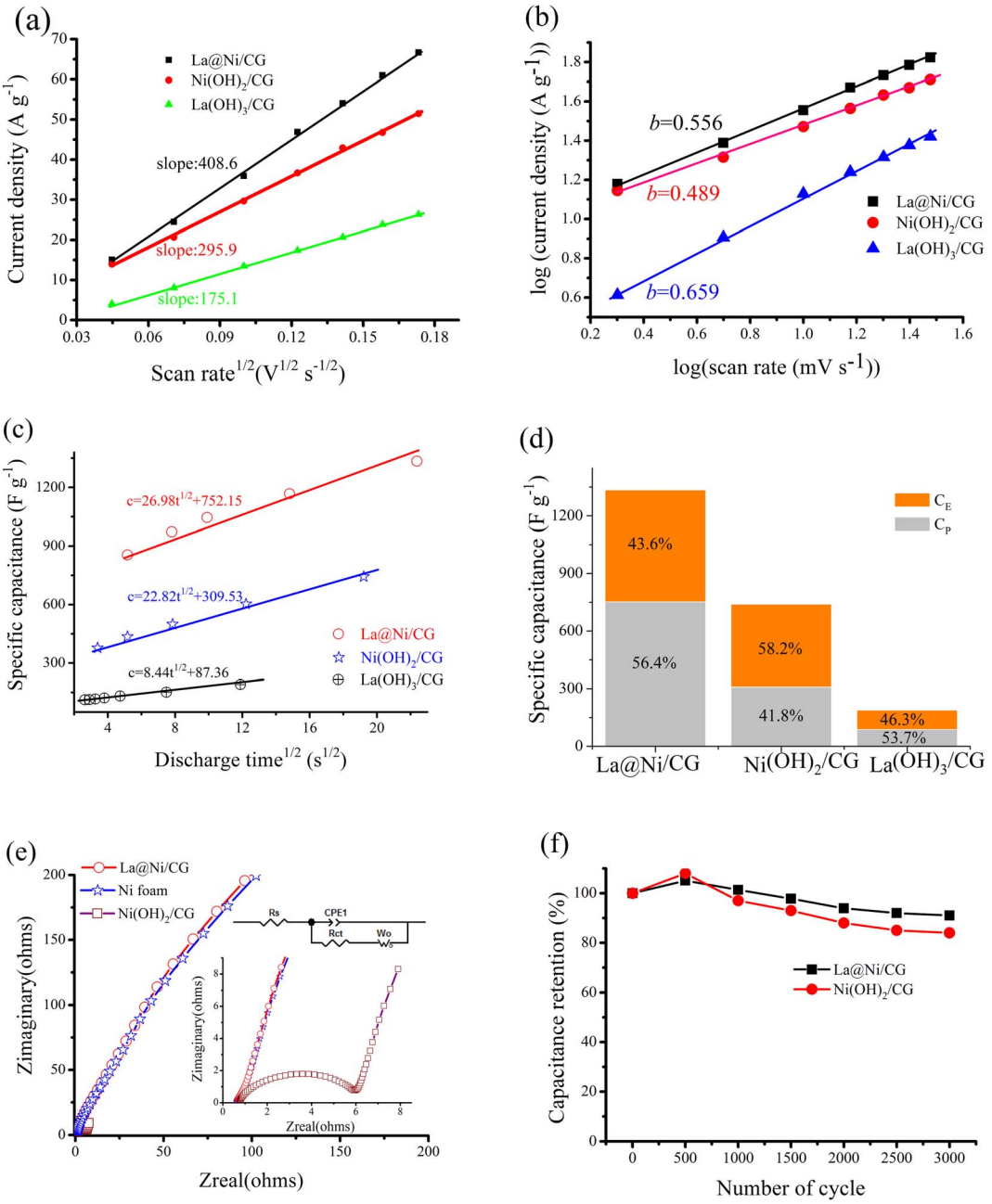


Fig. 6 (a) The linear relationship between the anodic peak current and the square root of the scan rate ($\nu^{1/2}$); (b) determine the $b$-value by relating the peak current to the scanning rate according to the voltammograms; (c) specific capacitance *vs.* $t^{1/2}$; (d) EDLCs and faradaic pseudocapacitor contributions from specimens; (e) Nyquist plot of Ni foam, $Ni(OH)_2$ and La@Ni/CG electrodes at frequencies from 100 kHz to 0.01 Hz; (f) cycle performance of La@Ni/CG at a current density of 2 A $g^{-1}$ in 3 M KOH solution.

composite have a linear relationship, indicating that the reaction is diffusion controlled. This behavior is consistent with the Randles–Sevcik formula, which describes the behavior of electrochemical reactions under diffusion control. The statement implies that the composite behaves in a predictable and consistent manner according to the established electrochemical principles. The plot can be used to determine the ion diffusion coefficient of $La(OH)_3$/CG, $Ni(OH)_2$/CG and La@Ni/CG. The slope of La@Ni/CG is greater than that of $La(OH)_3$/CG and $Ni(OH)_2$/CG, indicating a higher ion diffusion coefficient for La@Ni/CG due to its unique structure. This suggests that La@Ni/CG may be more efficient in ion diffusion than the other materials.

The charge storage kinetics of the electrode materials for ions were studied by CV analysis. The power law relationship $i = a\nu^b$ is assumed for the current ($i$) and the scan rate ($\nu$), where $a$ and $b$ are adjustable parameters. $a$ and $b$ value of 0.5 indicates diffusion controlled behavior, while the value of 1.0 indicates capacitive process.[42] The value can be determined from the slope of Fig. 6b. The results show that $La^{3+}$ increases the value of $b$ of the material from 0.489 to 0.556, which offers

Open Access Article. Published on 19 July 2023. Downloaded on 1/12/2026 11:23:45 PM. This article is licensed under a Creative Commons Attribution-NonCommercial 3.0 Unported Licence.

a positive contribution to the charge storage kinetics of La@Ni/CG. In general, the total capacitance ($C_T$) can be divided into two parts: the rate independent part $k_1$ (related to EDLC and CE) and the diffusion limited part $k_2t^{1/2}$ (due to faradaic pseudocapacitor, $C_P$), as described by the following equation.[43]

$$C_T = k_1 + k_2t^{1/2} \tag{8}$$

Fig. 6c shows the relationship between the $C_T$ and the square root of the discharge time. It is worth noting that the contribution of the EDLC and faradaic pseudocapacitor of $Ni(OH)_2$/CG to the total specific capacitance is 58.2% and 48.1%, respectively, while that of La@Ni/CG is 43.6% and 56.4% (Fig. 6d), showing that lanthanum makes a positive contribution to the faradaic pseudocapacitor of La@Ni/CG composite.

In summary, the addition of lanthanum to the $Ni(OH)_2$ increases the ion diffusion coefficient, which has a positive effect on the charge storage kinetics of the La@Ni/CG and increases its faradaic pseudocapacitor ratio. This is attributed to the alternating layer structure of Ni/La, which promotes electrolyte diffusion, delays polarization, and reduces the activation energy of the reaction. As a result, the addition of lanthanum exposes more active sites in La@Ni/CG, providing a conductive channel for consuming/generating electrons through the Faraday reaction, further improving its conductivity and providing a better pathway for ion transport.

Fig. 6e shows the analysis of Ni foam, $Ni(OH)_2$/CG, and La@Ni/CG using EIS to quantify the resistance at the electrode/electrolyte interface. The inset shows the expanded plots at high frequency and the equivalent circuit derived from the Nyquist plots, where $R_s$ is the bulk solution resistance, $R_{ct}$ is the faradaic interfacial charge transfer resistance, $CPE_1$ is the constant phase element taking into account the double layer capacitance, Wo is the Warburg impedance. By comparing the Nyquist diagram, it can be seen that the diameter of the semicircle of the $Ni(OH)_2$/CG, Ni foam and La@Ni/CG materials (the charge transfer resistance index, $R_{ct}$) is 5.2, 0.3 and 0.4 Ω, respectively. It can be seen that the addition of $La^{3+}$ is beneficial to the formation of the conductive network of La@Ni/CG, providing an abundance of mobile charge carriers and conductive channels, which is beneficial to the transfer of electrons. This result is consistent with that shown in Fig. 6a. In addition, the knee frequency at which the predominant capacitive behavior can be maintained is determined by the intersection of a Warburg-type line (inclined at 45°) and a low-frequency vertical line. The projection length on the real part ($Z'$) of the impedance axis reflects the ion penetration process, and it is obvious that the diffusion path of La@Ni/CG is shorter than that of $Ni(OH)_2$/CG. In addition, the cycle life measurement of binary composites at a current density of 2 A $g^{-1}$ is shown in Fig. 6f. After 3000 repeated cycles, La@Ni/CG can still provide the specific capacitance of 1159 F $g^{-1}$, and the capacitance retention is 90.6% of the initial value, indicating that the system has good reversible electrochemical activity.

# 4. Conclusions

In summary, the binary composite La@Ni/CG on carboxyl graphene was synthesized *via* a simple method. The resulting sample was used as the hybrid supercapacitor electrode with excellent electrochemical performance. The composite combines the high electrical conductivity of $Ni(OH)_2$/CG and the high surface area of $La(OH)_3$/CG with the excellent mechanical properties of carboxyl graphene. The binary composite has been shown to improve the electrical conductivity and cyclic stability of the material due to its intrinsic electrical and mechanical properties, which enabled $Ni(OH)_2$-based electrodes to be used in hybrid supercapacitor applications. The fabricated electrode had a capacitance retention of 90.6% after 3000 cycles. This cost-effective synthetic method can be used to other electroactive samples and offers promise for high energy storage devices.

# Author contributions

The authors contributed equally to this paper.

# Conflicts of interest

The authors declare no conflict of interest.

# Acknowledgements

The authors gratefully acknowledge the financial support from the National Natural Science Foundation of China (51377047), the Six Talent Peaks Project in Jiangsu Province (JNHB-220), Qing Lan Project of Jiangsu Higher Education of China and the 521 Engineering Program of Lianyungang (LYG06521202110).

# References

1 H. Zhang, D. Yang, A. Lau, T. Ma and B. Jia, Hybridized graphene for supercapacitors: Beyond the limitation of pure graphene, *Small*, 2021, **17**, 2007311, DOI: 10.1002/smll.202007311.

2 S. W. Bokhari, A. H. Siddique, P. C. Sherrell, X. Yue and W. Gao, Advances in graphene-based supercapacitor electrodes, *Energy Rep.*, 2020, **6**, 2768–2784, DOI: 10.1016/j.egyr.2020.10.001.

3 M. Khandelwal, C. VanTran, J. Lee and J. B. In, Nitrogen and boron co-doped densified laser-induced graphene for supercapacitor applications, *Chem. Eng. J.*, 2022, **428**, 131119, DOI: 10.1016/j.cej.2021.131119.

4 A. Méndez-Reséndiz, U. A. Méndez-Romero, R. A. Mendoza-Jiménez, B. A. Abdulahi, S. A. Pérez-García, E. Wang and L. Licea-Jiménez, Highly crystalline selectively oxidized graphene for supercapacitors, *FlatChem*, 2023, **38**, 100483, DOI: 10.1016/j.flatc.2023.100483.

5 R. P. Priya, A. Baradeswaran and A. Bagubali, Energy storage improvement of graphene based super capacitors, *Mater.*

 © 2023 The Author(s). Published by the Royal Society of Chemistry

Open Access Article. Published on 19 July 2023. Downloaded on 1/12/2026 11:23:45 PM. This article is licensed under a Creative Commons Attribution-NonCommercial 3.0 Unported Licence.

*Today: Proc.*, 2023, **78**, 919–923, DOI: 10.1016/j.matpr.2023.02.279.

6 M. Aghazadeh, A. N. Golikand and M. Ghaemi, Synthesis, characterization, and electrochemical properties of ultrafine β-$Ni(OH)_2$ nanoparticles, *Int. J. Hydrogen Energy*, 2011, **36**, 8674–8679, DOI: 10.1016/j.ijhydene.2011.03.144.

7 G. S. Gund, D. P. Dubal, S. B. Jambure, S. S. Shinde and C. D. Lokhande, Temperature influence on morphological progress of $Ni(OH)_2$ thin films and its subsequent effect on electrochemical supercapacitive properties, *J. Mater. Chem. A*, 2013, **1**, 4793–4803, DOI: 10.1039/C3TA00024A.

8 Y. Wang, Y. Liang, D. Zeng, M. Zhu, J. Fu, T. Zhu, H. Han, C. Li and W. Wang, Electrochemical deposition of p-type β-$Ni(OH)_2$ nanosheets onto CdS nanorod array photoanode for enhanced photoelectrochemical water splitting, *Electrochim. Acta*, 2020, **337**, 135763, DOI: 10.1016/j.electacta.2020.135763.

9 E. C. Cho, C. W. Chang-Jian, K. C. Lee, J. H. Huang, B. C. Ho, R. Z. Liu and Y. S. Hsiao, Ternary composite based on homogeneous $Ni(OH)_2$ on graphene with Ag nanoparticles as nanospacers for efficient supercapacitor, *Chem. Eng. J.*, 2018, **334**, 2058–2067, DOI: 10.1016/j.cej.2017.11.175.

10 J. Li, C. Wei, Y. Sun, Q. Liu, X. Zhang and J. Guo, Hierarchical $Ni(OH)_2$-$MnO_2$ Array as Supercapacitor Electrode with High Capacity, *Adv. Mater. Interfaces*, 2019, **6**, 1801470, DOI: 10.1002/admi.201801470.

11 C. Wei, J. Sun, Y. Zhang, Y. Liu, Z. Guo and W. Du, Hierarchical $Ni(OH)_2$–$MnO_2$ hollow spheres as an electrode material for high-performance supercapacitors, *Inorg. Chem. Front.*, 2022, **9**, 3542–3551, DOI: 10.1039/D2QI00780K.

12 T. Nguyen, M. Boudard, M. J. Carmezim and M. F. Montemor, Layered $Ni(OH)_2$-$Co(OH)_2$ films prepared by electrodeposition as charge storage electrodes for hybrid supercapacitors, *Sci. Rep.*, 2017, **7**, 39980, DOI: 10.1038/srep39980.

13 J. A. Syed, J. Ma, B. Zhu, S. Tang and X. Meng, Hierarchical Multicomponent Electrode with Interlaced $Ni(OH)_2$ Nanoflakes Wrapped Zinc Cobalt Sulfide Nanotube Arrays for Sustainable High-Performance Supercapacitors, *Adv. Energy Mater.*, 2017, **7**, 1701228, DOI: 10.1002/aenm.201701228.

14 J. Huang, T. Lei, X. Wei, X. Liu, T. Liu, D. Cao, J. Yin and G. Wang, Effect of Al-doped β-$Ni(OH)_2$ nanosheets on electrochemical behaviors for high performance supercapacitor application, *J. Power Sources*, 2013, **232**, 370–375, DOI: 10.1016/j.jpowsour.2013.01.081.

15 Y. Zhu, S. An, X. Sun, J. Cui, Y. Zhang and W. He, Flower-like Y-doped α-$Ni(OH)_2$/graphene heterostructure as advanced electrodes for high performance supercapacitor, *Vacuum*, 2020, **172**, 109055, DOI: 10.1016/j.vacuum.2019.109055.

16 M. P. Harikrishnan, A. J. C. Mary and A. C. Bose, Electrochemical performance of $ANiO_3$ (A= La, Ce) perovskite oxide material and its device performance for supercapattery application, *Electrochim. Acta*, 2020, **362**, 137095, DOI: 10.1016/j.electacta.2020.137095.

17 Z. Tang, C. Tang and H. Gong, A high energy density asymmetric supercapacitor from nano-architectured $Ni(OH)_2$/carbon nanotube electrodes, *Adv. Funct. Mater.*, 2012, **22**, 1272–1278, DOI: 10.1002/adfm.201102796.

18 R. R. Salunkhe, J. Lin, V. Malgras, S. X. Dou, J. H. Kim and Y. Yamauchi, Large-scale synthesis of coaxial carbon nanotube/$Ni(OH)_2$ composites for asymmetric supercapacitor application, *Nano Energy*, 2015, **11**, 211–218, DOI: 10.1016/j.nanoen.2014.09.030.

19 R. Ranjithkumar, S. E. Arasi, P. Devendran, N. Nallamuthu, P. Lakshmanan, S. Sudhahar, A. Arivarasan and M. K. Kumar, Investigations and fabrication of $Ni(OH)_2$ encapsulated carbon nanotubes nanocomposites based asymmetrical hybrid electrochemical supercapacitor, *J. Energy Storage*, 2020, **32**, 101934, DOI: 10.1016/j.est.2020.101934.

20 W. S. Li, Y. C. Shih and H. C. Cheng, Green synthesis of CNTs/$Ni(OH)_2$ nanostructures for electrochemical supercapacitors, *Chem. Phys. Lett.*, 2020, **750**, 137499, DOI: 10.1016/j.cplett.2020.137499.

21 Y. Xu, X. Huang, Z. Lin, X. Zhong, Y. Huang and X. Duan, One-step strategy to graphene/$Ni(OH)_2$ composite hydrogels as advanced three-dimensional supercapacitor electrode materials, *Nano Res.*, 2013, **6**, 65–76, DOI: 10.1007/s12274-012-0284-4.

22 J. Yan, Z. Fan, W. Sun, G. Ning, T. Wei, Q. Zhang, R. Zhang, L. Zhi and F. Wei, Advanced Asymmetric Supercapacitors Based on $Ni(OH)_2$/Graphene and Porous Graphene Electrodes with High Energy Density, *Adv. Funct. Mater.*, 2012, **22**, 2632–2641, DOI: 10.1002/adfm.201102839.

23 B. Guo, Y. Gao, Y. Li, X. Sun, S. Chen and M. Li, $Ni(OH)_2$ Nanosheets Grown on Reduced Graphene Oxide for Supercapacitor Electrodes, *ACS Appl. Nano Mater.*, 2022, **5**, 7471–7480, DOI: 10.1021/acsanm.2c01464.

24 Y. Zhao, L. Hu, S. Zhao and L. Wu, Preparation of $MnCo_2O_4$@$Ni(OH)_2$ Core–Shell Flowers for Asymmetric Supercapacitor Materials with Ultrahigh Specific Capacitance, *Adv. Funct. Mater.*, 2016, **26**, 4085–4093, DOI: 10.1002/adfm.201600494.

25 S. Uppugalla and P. Srinivasan, Polyaniline nanofibers and porous $Ni(OH)_2$ sheets coated carbon fabric for high performance super capacitor, *J. Appl. Polym. Sci.*, 2019, **136**, 48042, DOI: 10.1002/app.48042.

26 F. Wolfart, D. P. Dubal, M. Vidotti and P. Gómez-Romero, Hybrid core–shell nanostructured electrodes made of polypyrrole nanotubes coated with $Ni(OH)_2$ nanoflakes for high energy-density supercapacitors, *RSC Adv.*, 2016, **6**, 15062–15070, DOI: 10.1039/C5RA23671A.

27 R. Jafer, S. A. Alsufyani, J. Iqbal, M. O. Ansari, A. Numan, S. Bashir and S. Wageh, Silver decorated and graphene wrapped polypyrrole@$Ni(OH)_2$ quaternary nanocomposite for high performance energy storage devices, *Polymers*, 2023, **15**, 1267, DOI: 10.3390/polym15051267.

28 X. Liu, G. Du, J. Zhu, Z. Zeng and X. Zhu, NiO/$LaNiO_3$ film electrode with binder-free for high performance supercapacitor, *Appl. Surf. Sci.*, 2016, **384**, 92–98, DOI: 10.1016/j.apsusc.2016.05.005.

29 D. Han, X. Jing, J. Wang, P. Yang, D. Song and J. Liu, Porous lanthanum doped NiO microspheres for supercapacitor

Open Access Article. Published on 19 July 2023. Downloaded on 1/12/2026 11:23:45 PM.
This article is licensed under a Creative Commons Attribution-NonCommercial 3.0 Unported Licence.

application, *J. Electroanal. Chem.*, 2012, **682**, 37–44, DOI: 10.1016/j.jelechem.2012.06.016.

30 J. Jia, F. Luo, C. Gao, C. Suo, X. Wang, H. Song and X. Hu, Synthesis of La-doped NiO nanofibers and their electrochemical properties as electrode for supercapacitors, *Ceram. Int.*, 2014, **40**, 6973–6977, DOI: 10.1016/j.ceramint.2013.12.024.

31 X. W. Wang, Q. Q. Zhu, X. E. Wang, H. C. Zhang, J. J. Zhang and L. F. Wang, Structural and electrochemical properties of $La_{0.85}Sr_{0.15}MnO_3$ powder as an electrode material for supercapacitor, *J. Alloys Compd.*, 2016, **675**, 195–200, DOI: 10.1016/j.jallcom.2016.03.048.

32 D. Zheng, R. Yao, C. Sun, Y. Zheng and C. Liu, Highly efficient low-concentration phosphate removal from effluents by recoverable $La(OH)_3$/foamed nickel adsorbent, *ACS Omega*, 2021, **6**, 5399–5407, DOI: 10.1021/acsomega.0c05489.

33 P. Bocchetta, M. Santamaria and F. D. Quarto, Template electrosynthesis of $La(OH)_3$ and $Nd(OH)_3$ nanowiresusing porous anodic alumina membranes, *Electrochem. Commun.*, 2007, **9**, 683–688, DOI: 10.1016/j.elecom.2006.10.053.

34 A. Subasri, K. Balakrishnan, E. R. Nagarajan, V. Devadoss and A. Subramania, Development of 2D $La(OH)_3$/graphene nanohybrid by a facile solvothermal reduction process for high-performance supercapacitors, *Electrochim. Acta*, 2018, **281**, 329–337, DOI: 10.1016/j.electacta.2018.05.142.

35 S. I. Kim, J. S. Lee, H. J. Ahn, H. K. Song and J. H. Jang, Facile route to an efficient NiO supercapacitor with a three-dimensional nanonetwork morphology, *ACS Appl. Mater. Interfaces*, 2013, **5**, 1596–1603, DOI: 10.1021/am3021894.

36 J. Liu, J. Wang, Y. Fo, B. Zhang, C. Molochas, J. Gao, W. Li, X. Cui, X. Zhou, L. Jiang and P. Tsiakaras, Engineering of unique Ni-Ru nano-twins for highly active and robust bifunctional hydrogen oxidation and hydrogen evolution electrocatalysis, *Chem. Eng. J.*, 2023, **454**, 139959, DOI: 10.1016/j.cej.2022.139959.

37 T. Zheng, K. Jiang, N. Ta, Y. Hu, J. Zeng, J. Liu and H. Wang, Large-scale and highly selective $CO_2$ electrocatalytic reduction on nickel single-atom catalyst, *Joule*, 2019, **3**, 265–278, DOI: 10.1016/j.joule.2018.10.015.

38 G. Shao, Y. Yao, S. Zhang and P. He, Supercapacitor characteristic of La-doped $Ni(OH)_2$ prepared by electrodeposition, *Rare Met.*, 2009, **28**, 132–136, DOI: 10.1007/s12598-009-0026-2.

39 Z. M. Riyas, C. Priya, R. Premila, G. Maheshwaran, S. Sudhahar and M. R. Prabhu, Synergistic effect of $La_2O_3$-NiO nanocomposite based electrode for electrochemical high-performance asymmetric supercapacitor applications, *J. Energy Storage*, 2022, **53**, 104988, DOI: 10.1016/j.est.2022.104988.

40 L. Hu, Y. Deng, K. Liang, X. Liu and W. Hu, $LaNiO_3$/NiO hollow nanofibers with mesoporous wall: a significant improvement in NiO electrodes for supercapacitors, *J. Solid State Electrochem.*, 2015, **19**, 629–637, DOI: 10.1007/s10008-014-2641-6.

41 G. Wang, K. Qi, Z. Yan, L. Yue, Y. Ding, W. Li and Z. Xu, Microwave hydrothermal synthesis of La decorated $Ni(OH)_2$ nanosheets for performance-enhanced hybrid supercapacitor, *Appl. Surf. Sci.*, 2022, **592**, 153293, DOI: 10.1016/j.apsusc.2022.153293.

42 M. Guo, Y. Liu, F. Zhang, F. Cheng, C. Cheng, Y. Miao, G. Feng and J. Yu, Inactive $Al^{3+}$-doped $La(CoCrFeMnNiAl_x)_{1/(5+x)}O_3$ high-entropy perovskite oxides as high performance supercapacitor electrodes, *J. Adv. Ceram.*, 2022, **11**, 742–753, DOI: 10.1007/s40145-022-0568-4.

43 X. Sun, Z. Meng, Z. Hao, Z. Du, J. Xu, H. Nan, W. Shi, F. Zeng, X. Hu and H. Tian, Efficient fabrication of flower-like core–shell nanochip arrays of lanthanum manganate and nickel cobaltate for high-performance supercapacitors, *J. Colloid Interface Sci.*, 2023, **630**, 618–628, DOI: 10.1016/j.jcis.2022.10.035.

44 Z. Hao, Z. Meng, X. Li, X. Sun, J. Xu, H. Nan, W. Shi, G. Qi, X. Hu and H. Tian, Two-step fabrication of lanthanum nickelate and nickel oxide core-shell dandelion-like materials for high-performance supercapacitors, *J. Colloid Interface Sci.*, 2022, **617**, 430–441, DOI: 10.1016/j.jcis.2022.03.001.

 © 2023 The Author(s). Published by the Royal Society of Chemistry